Nanoscale

On the Role of Ligands in Atomically Precise Nanocluster-Catalyzed CO2 Electrochemical Reduction

Journal:	*Nanoscale*
Manuscript ID	NR-COM-11-2020-007832.R1
Article Type:	Communication
Date Submitted by the Author:	21-Dec-2020

Complete List of Authors:	Li, Site; Carnegie Mellon University, Chemistry Nagarajan, Anantha ; University of Pittsburgh, Chemical and Petroleum Engineering Li, Yingwei; Carnegie Mellon University, Chemistry; Shanghai Normal University, Mathematics and physics Kauffman, Douglas; National Energy Technology Laboratory, United States Department of Energy Mpourmpakis, Giannis; University of Pittsburgh, Chemical and Petroleum Engineering Jin, Rongchao; Carnegie Mellon University, Chemistry

COMMUNICATION

On the Role of Ligands in Atomically Precise Nanocluster-Catalyzed CO_2 Electrochemical Reduction

Received 00th January 20xx,
Accepted 00th January 20xx

DOI: 10.1039/x0xx00000x

Site Li,[a,b,†] Anantha Venkataraman Nagarajan,[c,†] Yingwei Li,[a] Douglas R. Kauffman,*[b] Giannis Mpourmpakis,*[c] and Rongchao Jin*[a]

Ligand effects are of major interest in catalytic reactions owing to their potential critical role in determining the reaction activity and selectivity. Herein, we report ligand effects in CO_2 electrochemical reduction reaction at the atomic level with three unique Au_{25} nanoclusters comprising the same kernel but different protecting ligands (-XR, where X = S or Se, and R represents the carbon tail). It is observed that a change in carbon tail shows no obvious impact on the catalytic selectivity and activity, but the anchoring atom (X = S or Se) strongly affects the electrocatalytic selectivity. Specifically, the S site acts as the active site and sustains CO selectivity, while the Se site shows a higher tendency of hydrogen evolution. Density functional theory (DFT) calculations reveal that the energy penalty associated with COOH formation is lower on the S site by 0.26 eV compared to the Se site. Additionally, the formation energy of the product (*CO) is lower on the sulfur-based Au nanocluster by 0.43 eV. We attribute these energetic differences to the higher electron density on the sulfur sites of the Au nanocluster, resulting in modified bonding character of the reaction intermediates that reduce the energetic penalty for COOH and *CO formation. Overall, this work demonstrates that S/Se atoms at the metal-ligand interface can play an important role in determining the overall electrocatalytic performance of Au nanoclusters.

Electrochemical reduction of carbon dioxide (CO_2RR) is under intensive research as a route to convert CO_2 into value-added chemicals and fuels.[1,2] Among the catalysts, metal nanoparticles have been extensively studied owing to their high activity, high conductivity and stability during the electrochemical operation.[3,4] The key factors determining the catalytic performance of metal nanoparticles include the doping effects,[5,6] size effects[7, 8] and ligand effects[9-14]. However, as is known, the inhomogeneities of regular nanoparticles in size, composition, morphology, and crystallographic facets often obscure the underlying structure-property relationships in fundamental research.[2] The case of ligand-protected nanoparticles is particularly challenging because it is difficult to obtain realistic models for complementary density functional theory (DFT) studies. In this context, it is highly desirable to create atomically precise nanoparticles with specific number of metal atoms and ligands for mechanistic studies.[2,15-21]

Using atomically precise metal nanoparticles (often called nanoclusters) is advantageous, as such nanoclusters eliminate the concerns on the inhomogeneities, and more importantly, their ultrasmall size (1-2 nm) also removes the material gap between experiments and theoretical modelling,[2] thus, such nanoclusters hold great promise in fundamental catalysis research. Ligand-protected Au nanoclusters can be represented as $Au_n(XR)_m$, where n and m stand for the exact number of Au atoms and protecting ligands, respectively, and X represents metal-binding atom such as S and Se. These nanoclusters consist of tens to hundreds of gold atoms and lie in the size regime from molecular-like to plasmonic nanoparticles.[22,23] With the atomic-level structures and tailored ligands,[23] Au nanoclusters are promising systems to study the ligand effects. DFT calculations based on the crystal structures can bridge the structure and catalytic properties by providing insights into the electronic effects from the presence of ligands and nanocluster morphology.[26-29]

Here, we investigate the ligand effects at the atomic level with three unique $[Au_{25}(XR)_{18}]^-$ nanoclusters protected by different ligands, namely, 2-phenylethanethiolate (PET), 1-naphthalenethiolate (Nap) and benzeneselenolate (SePh). The critical role of the ligand's head group (X = S or Se) is identified, whereas the carbon tail of the ligand shows no major impact on the reactivity. DFT calculations also elucidate the active site and overall reaction energetics.

[a] Department of Chemistry, Carnegie Mellon University, Pittsburgh, Pennsylvania 15213, USA. Email: rongchao@andrew.cmu.edu
[b] National Energy Technology Laboratory (NETL), United States Department of Energy, Pittsburgh, Pennsylvania, USA. Email: gmpourmp@pitt.edu
[c] Department of Chemical Engineering, University of Pittsburgh, Pittsburgh, Pennsylvania 15261, United States. Email: Kauffman@NETL.DOE.GOV
† Contribute equally.

Electronic Supplementary Information (ESI) available: [details of any supplementary information available should be included here]. See DOI: 10.1039/x0xx00000x

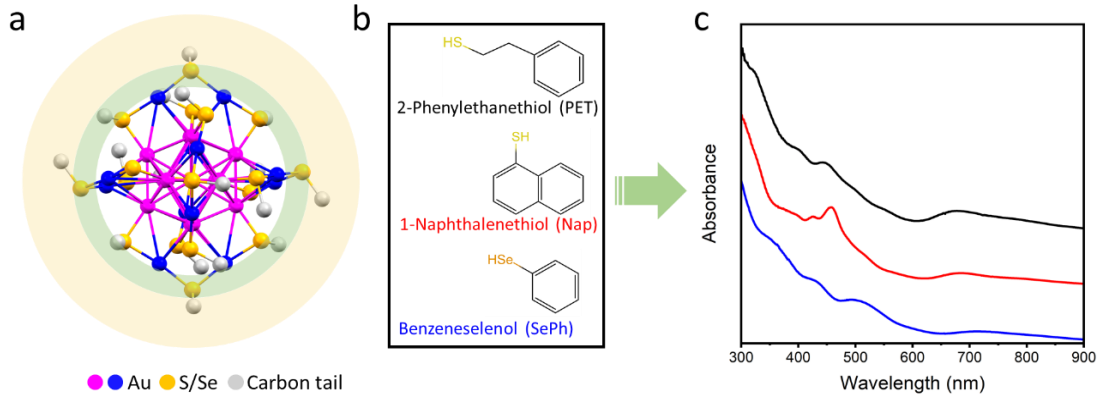

Figure 1. The structure and UV-vis spectra of Au nanoclusters. (a) Atom packing structures of Au_{25}. The light-green ring represents the ligand modification at kernel/ligand interface atoms, while the light-yellow ring represents the ligand modification at carbon tails. (b) formulas of three ligands. (c) UV-vis spectra of three ligands.

The atomic-level structures of the three Au_{25} nanoclusters were previously solved by X-ray crystallography.[30-32] All the three share the same structure (**Figure 1a**). The kernel is composed of a 13-atom icosahedron, which is protected by six staple-like dimeric motifs involving S or Se atoms and organic (R) groups (i.e., -**X**R-**Au**-**X**R-**Au**-**X**R-, X = S/Se). Here, the XR ligands of the three Au_{25} nanoclusters are PET, Nap and SePh, respectively, **Figure 1b**. PET and Nap are both thiols, and Nap has a larger steric hindrance because of the direct sulfur-naphthalene bond and larger ring size. The SePh ligand shares a similar structure with Nap, except the former contains Se atom for binding to the metal atoms and a smaller ring of carbon tail. Their UV-vis spectra are presented in **Figure 1c**. For the two thiolate-protected Au_{25} nanoclusters, their spectra show similar features in the long-wavelength part (e.g. distinct absorption at 670 nm), but the shorter wavelength region (<600 nm) is affected by the specific ligand. For the SePh protected Au_{25}, the long wavelength peak redshifts to ~720 nm (vs. 670 nm for thiolated Au_{25}). This redshift can be explained by more extensive mixing of Au 6s and Se 4p orbitals compared to the S 3p case. Overall, these three Au_{25} nanoclusters possess the same kernel structure but different surface ligands, providing a unique opportunity for studying the ligand effect on CO_2RR at the atomic level.

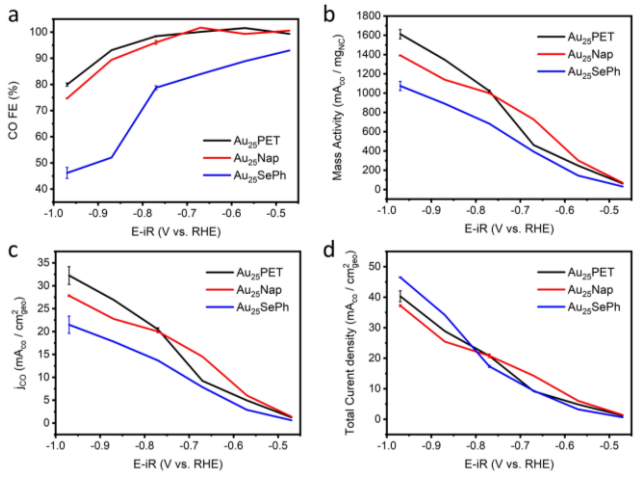

Figure 2. Electrocatalytic CO_2 reduction performance of various Au_{25} nanoclusters. (a) Faradaic Efficiency (FE) for CO production, (b) CO mass activity, (c) CO partial current density, and (d) Total current density (H_2 plus CO) over three Au_{25} nanoclusters.

The three nanoclusters were respectively deposited onto a carbon black support (Vulcan XC-72R), each at 10% weight loading for electrochemical testing. We note that carbon black is inert catalytically but it improves the electron transfer and thus facilitates CO_2RR. Electrocatalytic CO_2RR experiments showed that CO and H_2 were the only detected products. **Figure 2a** exhibits the potential-dependent Faradaic efficiency (FE) for CO production. The PET and Nap protected Au_{25} nanoclusters show a similar CO selectivity in the potential range from -0.5 to -1.0 V (vs reversible hydrogen electrode, RHE), and the CO FE of the two thiolated Au_{25} nanoclusters are close to 100% at potentials smaller than -0.8 V. On the other hand, the SePh protected Au_{25} shows substantially lower CO FE across the entire potential range. These result shows that the reaction selectivity is not sensitive to the steric hindrance of these specific protecting ligands; however, the steric effects may become important for very bulky or long-chain (e.g. $SC_{12}H_{25}$) ligands.[6] Our results highlight how the interface atom impacts the product selectivity for nanoclusters protected by ligands.

Figure 2b and **c** show the mass activity and partial current density of CO formation. The SePh-protected Au_{25} exhibits lower activity that that of the thiolate-protected ones. At -1.0 V, the mass activity of SePh-protected Au_{25} is only ~70% that of the PET-protected Au_{25}. The comparison of hydrogen evolution reaction (HER) of these three nanoclusters (**Figure S1**) shows an opposite trend to CO_2RR, with the SePh-protected Au_{25} producing substantially more H_2 than thiolate-protected clusters at all potentials. It is noted that the FE for CO_2RR and HER of each nanocluster sums to ~100% FE, thus, no other process occurs. ^{1}H Nuclear magnetic resonance (NMR) spectra in **Figure S2** also verified CO and H_2 as the only products. The total current densities of the three nanoclusters are shown in **Figure 2d**. The three nanoclusters exhibit similar currents at all potentials, indicating that the differences in CO specific current.

The high stability of Au_{25} during electrochemical test was previously reported.[33] To further verify the stability of the

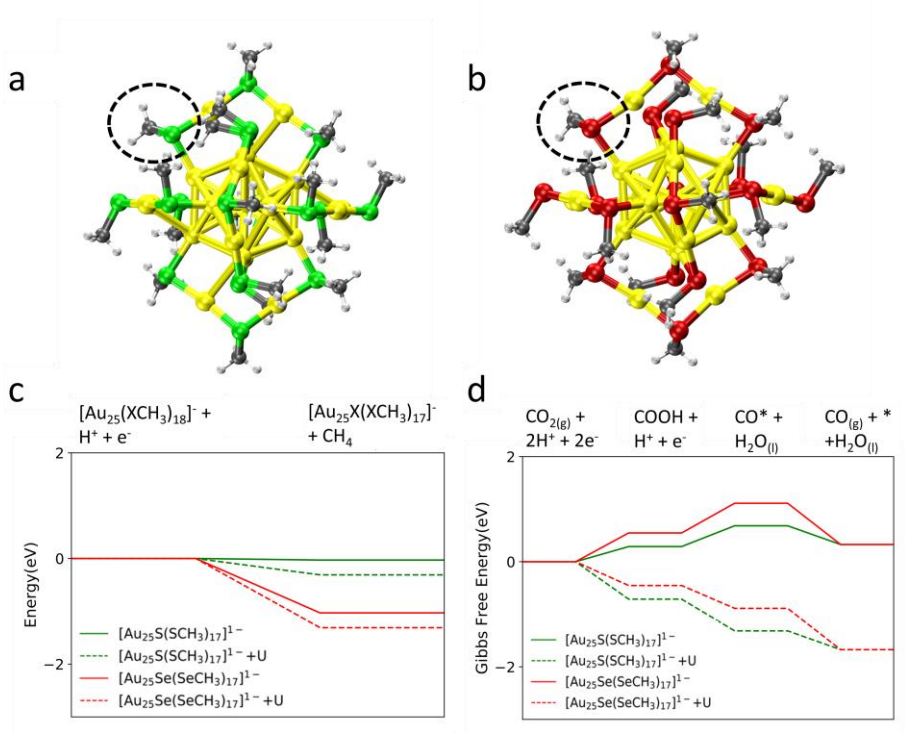

Figure 3. The relaxed structures of Au_{25} nanoclusters with (a) sulfur (-SCH_3) ligands and (b) selenium (-$SeCH_3$) ligands. Dotted circles represent the site of -R removal. Atom colors: Au: yellow, S: green, Se: red, C: grey, H: white. (c) Energy required for -R removal. (d) Energetics of CO_2RR pathway. X = S or Se. Dotted lines represent energy upon an applied voltage of U = -1.0 V. The asterisk (*) represents active site (S or Se atom).

three nanoclusters, UV-vis spectra before and after the catalytic reaction at -0.8 V for 10 min are provided in **Figure S3**. It can be seen that the spectral features retain after the electrochemical test, indicating high stability of these Au nanoclusters during the CO_2RR.

While in-situ real time studies on the CO_2RR mechanism is still challenging (e.g. active-site probing[2]) even though the Au_{25} catalysts are atomically precise, DFT modeling is highly feasible with the available structures of $Au_{25}(XR)_{18}$ and can thus provide valuable insights. Previous work has shown that, in order to be a highly active electrocatalyst, the Au_{25} nanocluster must lose one full ligand (-SR removal) or partial ligand (-R removal) to expose a catalytically active site[28,29,34,35]. Herein, the removal of the organic moiety of the ligand (-R) leads to exposure of a sulfur (or selenium) atom as active site, whereas the removal of an entire ligand (-XR) exposes a gold (Au) atom as active site. We note that the -R removal does not significantly change the UV-vis spectrum as evidenced by experimental observation and DFT calculations.[34,35] Moreover, the UV-Vis spectra do not change significantly when the reaction intermediates such as COOH, CO and H are present on the exposed sulfur active site of the nanocluster upon -R removal. Considering that the post-reaction sample can have an ensemble of different nanocluster states such as the ones mentioned above, we do not expect to observe major changes to the UV-Vis spectrum before and after the reaction (**Figure S2**).

The sulfur site has been shown to provide a more energetically favorable and selective pathway towards CO_2RR as compared to the Au site.[28] Thus, we choose to study the thermodynamics of -R removal that leads to the exposure of a sulfur (or selenium) active site. The relaxed structures of the Au_{25} nanoclusters (**Figure 3a** and **b**) with -SR/SeR ligands (R = CH_3 for reducing computational demands[36]) are similar to experimentally determined structures[30-32]. Owing to the symmetry of the Au_{25} nanocluster, there are two unique sites for -R removal that lead to S or Se active site exposure. The chosen site of ligand removal (dotted circles in **Figure 3a** and **b**) is the one from which the S/Se atom can be exposed with a lower energy penalty[28]. The -R removal (**Figure 3c**) is almost thermoneutral or exergonic for the S or Se based Au_{25} nanoclusters, respectively, implying that the formation of S/Se active sites is feasible under electrochemical reaction conditions (applied potential of -1.0 V). While the thermodynamic feasibility of exposing a sulfur active site is higher by 0.28 eV compared to a selenium active site, we expect the extent of formation of these active sites to be significant upon application of a potential of -1.0 V. Bader charge analysis (**Table S1**) reveals that upon ligand removal, the sulfur active site has a greater negative charge of -0.31|e| (implying higher electron density) compared to the selenium active site (-0.20|e|), suggesting potentially different interactions with reaction intermediates. Finally, comparable energies were required to remove the entire -SR (1.15 eV) or -SeR (1.22 eV) ligand and expose an Au active site. These energy barriers suggest the electrocatalytic active sites to be S or Se atoms.

While assessing the first step (COOH formation) of the CO_2RR pathway (**Figure 3d**), we observe significant energy differences between the sulfur-based Au_{25} nanocluster (S-Au_{25})

Table 1. Limiting step and corresponding potential of CO_2RR and HER on S-Au_{25} and Se-Au_{25} nanoclusters upon -R removal. $H^+ + e^-$ omitted in steps for simplicity.

	CO_2 RR	$U_{L, CO2}$	HER	$U_{L, H2}$	$U_{L, CO2} - U_{L, H2}$
$Au_{25\text{-sulfur}}$	*COOH → *CO + H_2O	-0.40 V	*H → $H_{2(g)}$ + *	-0.62 V	0.22 V
$Au_{25\text{-selenium}}$	*COOH → *CO + H_2O	-0.56 V	*H → $H_{2(g)}$ + *	-0.28 V	-0.28 V

and the selenium-based Au_{25} nanocluster (Se-Au_{25}). This is a crucial step in the reaction pathway and is energetically more feasible by 0.26 eV on S-Au_{25} as compared to the Se-Au_{25}. The favorable formation of COOH can be attributed to the higher electronic density on the S active site compared to the Se active site, stabilizing the COOH intermediate. The localized electron density on the S active sites of Au nanoclusters has been previously shown to affect the COOH stabilization step.[28] Analysis of the highest occupied molecular orbital (HOMO) and lowest unoccupied molecular orbital (LUMO) of S-Au_{25} and Se-Au_{25} upon COOH adsorption (**Figure S4**) reveals greater contribution of COOH orbitals to the frontier orbitals of S-Au_{25} compared to Se-Au_{25}. Additionally, the HOMO of Se-Au_{25} upon COOH adsorption shows a minimal contribution of COOH orbitals to the frontier orbitals of the nanocluster, signifying that COOH is more reactive when it is adsorbed on the S active site instead of the Se active site. By noting the greater contribution of COOH orbitals to S-Au_{25}, we observe that the *CO intermediate is more stable on the sulfur active site than selenium by 0.43 eV, indicating a lower thermodynamic barrier for the formation of *CO (step 2 in the reaction pathway) on the S-Au_{25} as compared to the Se-Au_{25}.

The HER competes with CO_2RR at the experimentally applied potentials used in this work.[37, 38] In order to assess the selectivity of the two systems (S-Au_{25} and Se-Au_{25}) towards CO_2RR and HER, we compared the minimum energy required (known as limiting potential 'U_L') to drive all reaction steps downhill for each reaction. It is worth noting the strong binding energy of *H on S-Au_{25} (-0.62 eV) compared to Se-Au_{25} (-0.28 eV). As a result, more energy is required (0.34 eV) for *H desorption on S-Au_{25}, thus demonstrating higher HER activity on Se-Au_{25} than S-Au_{25} (**Figure S5**). Bader charge analysis reveals that the electronic charge on H adsorbed on S-Au_{25} is higher (-1.15 |e|) than when it is on Se-Au_{25} (-0.99|e|), suggesting greater electronic interaction of H with the sulfur active site than selenium. The limiting potential for HER ($U_{L, H2}$) is $H_{2(g)}$ formation, while the limiting potential for CO_2RR ($U_{L, CO2}$) is *CO formation on both nanoclusters. The difference between the two limiting potentials (ΔU_L) provides us with qualitative information on the selectivity of each system towards CO_2RR or HER. The difference in limiting potentials for S-Au_{25} is substantially more positive (0.22 eV) than Se-Au_{25} (-0.28 eV), suggesting that the former is more selective towards CO formation as compared to $H_{2(g)}$ formation (for details see **Table 1**). This is consistent with the experimental observation of lower FE for CO (**Figure 2a**) on Se-Au_{25} compared to S-Au_{25}.

Overall, computational results elucidate the crucial role of interfacial S/Se atoms in affecting the CO_2RR selectivity, which is consistent with experimental observations of higher selectivity on S-Au_{25} towards CO_2RR than on Se-Au_{25}. Of note, one should not ignore the role of the underlying gold kernel in rendering the S/Se catalytic differences, because the S/Se active sites are strongly bonded to the gold core after all, including the charge transfer from gold and electron reservoir role of the gold kernel, not to mention the high conductivity of the gold kernel. Thus, it is the combined S-Au_{25} (or Se-Au_{25}) that leads to the unique catalytic behavior.

In summary, we have studied the ligand effects by comparing three Au_{25} nanoclusters with different ligands. The change in bulkiness of the protecting ligands shows no major impact on the catalytic selectivity, while the ligand's head (X = S/Se) exhibits strong influences on both selectivity and activity. Through first principles calculations, we attribute the higher selectivity of thiolate-protected nanoclusters to the higher electronic interaction of adsorbates with the exposed S active site compared to the Se site in selenolate-protected nanoclusters. An increase in the electron density on the S-sites of the nanocluster results in modified bonding character of the reaction intermediates that reduce the energetic penalty for COOH and CO. Apparently, such insights would not be possible to obtain without atomically precise nanoclusters. Thus, using nanoclusters as model catalysts in mechanistic studies is highly valuable, which will provide insights for tailoring the nanocluster catalysts toward highly active and selective electrocatalysts. Additionally, the ligand effect study based on Au nanoclusters can also provide insights into other metal nanoclusters, e.g., alloy and copper nanoclusters.

Conflicts of interest

There are no conflicts to declare.

Acknowledgements

The support of the U.S. Department of Energy, National Energy Technology Laboratory through NETL-Penn State University Coalition for Fossil Energy Research (UCFER, contract number DE-FE0026825) is gratefully acknowledged. The authors would like to acknowledge computational support from the Center for Research Computing at the University of Pittsburgh, the National Energy Research Scientific Computing Center (NERSC), a U.S. Department of Energy Office of Science User Facility operated under Contract No. DE-AC02-05CH11231 and the Extreme Science and Engineering Discovery Environment, which is supported by the NSF (ACI-1548562). This report was prepared as an account of work sponsored by an agency of the United States Government. Neither the United States Government nor any agency thereof, nor any of their employees, makes any warranty, express or implied, or assumes any legal liability or responsibility for the accuracy, completeness, or usefulness of any information, apparatus, product, or process disclosed, or represents that its use would not infringe privately owned rights. Reference therein to any specific commercial product, process, or service by trade name, trademark, manufacturer, or otherwise does not necessarily constitute or imply its endorsement, recommendation, or favoring by the United States Government or any agency

thereof. The views and opinions of authors expressed therein do not necessarily state or reflect those of the United States Government or any agency thereof.

References

1. C. Costentin, M. Robert and J.-M. Savéant, *Chem. Soc. Rev.*, 2013, **42**, 2423-2436.
2. R. Jin, G. Li, S. Sharma, Y. Li and X. Du, *Chem. Rev.*, 2020, doi: 10.1021/acs.chemrev.0c00495.
3. S. Zhao, R. Jin and R. Jin, *ACS Energy Lett.*, 2018, **3**, 452-462.
4. J. Kim, J. T. Song, H. Ryoo, J.-G. Kim, S.-Y. Chung and J. Oh, *J. Mater. Chem. A*, 2018, **6**, 5119-5128.
5. D. Kim, J. Resasco, Y. Yu, A. M. Asiri and P. Yang, *Nat. Commun.*, 2014, **5**, 4948.
6. B. Kumar, T. Kawawaki, N. Shimizu, Y. Imai, D. Suzuki, S. Hossain, L. V. Nair and Y. Negishi, *Nanoscale*, 2020, **12**, 9969-9979.
7. R. Reske, H. Mistry, F. Behafarid, B. Roldan Cuenya and P. Strasser, *J. Am. Chem. Soc.*, 2014, **136**, 6978-6986.
8. P. Iyengar, J. Huang, G. L. De Gregorio, C. Gadiyar and R. Buonsanti, *Chem. Commun.*, 2019, **55**, 8796-8799.
9. Z. Cao, D. Kim, D. Hong, Y. Yu, J. Xu, S. Lin, X. Wen, E. M. Nichols, K. Jeong and J. A. Reimer, *J. Am. Chem. Soc.*, 2016, **138**, 8120-8125.
10. S. Dou, J. Song, S. Xi, Y. Du, J. Wang, Z. F. Huang, Z. J. Xu and X. Wang, *Angew. Chem.*, 2019, **131**, 4081-4085.
11. F. Li and Q. Tang, *J. Mater. Chem. A*, 2019, **7**, 19872-19880.
12. R. R. Nasaruddin, Q. Yao, T. Chen, M. J. Hülsey, N. Yan and J. Xie, *Nanoscale*, 2018, **10**, 23113-23121.
13. M. Cui, G. Johnson, Z. Zhang, S. Li, S. Hwang, X. Zhang and S. Zhang, *Nanoscale*, 2020, **12**, 14068-14075.
14. J. R. Pankhurst, P. Iyengar, A. Loiudice, M. Mensi and R. Buonsanti, *Chem. Sci*, 2020, **11**, 9296-9302.
15. T. Higaki, Y. Li, S. Zhao, Q. Li, S. Li, X. S. Du, S. Yang, J. Chai and R. Jin, *Angew. Chem.*, 2019, **131**, 8377-8388.
16. O. J. H. Chai, Z. Liu, T. Chen and J. Xie, *Nanoscale*, 2019, **11**, 20437-20448.
17. M. Muzzio, J. Li, Z. Yin, I. M. Delahunty, J. Xie and S. Sun, *Nanoscale*, 2019, **11**, 18946-18967.
18. M. Liu and W. Chen, *Nanoscale*, 2013, **5**, 12558-12564.
19. Q. Wang, L. Wang, Z. Tang, F. Wang, W. Yan, H. Yang, W. Zhou, L. Li, X. Kang and S. Chen, *Nanoscale*, 2016, **8**, 6629-6635.
20. S. Li and R. Jin, in *Recent Advances in Nanoparticle Catalysis*, Springer, 2020, pp. 39-68.
21. S. Wang, H. Yu and M. Zhu, *Sci. China Chem.*, 2016, **59**, 206-208.
22. T. Higaki, M. Zhou, K. J. Lambright, K. Kirschbaum, M. Y. Sfeir and R. Jin, *J. Am. Chem. Soc.*, 2018, **140**, 5691-5695.
23. R. Jin, C. Zeng, M. Zhou and Y. Chen, *Chem. Rev.*, 2016, **116**, 10346-10413.
24. S.-S. Zhang, L. Feng, R. D. Senanayake, C. M. Aikens, X.-P. Wang, Q.-Q. Zhao, C.-H. Tung and D. Sun, *Chem. Sci*, 2018, **9**, 1251-1258.
25. S.-S. Zhang, R. D. Senanayake, Q.-Q. Zhao, H.-F. Su, C. M. Aikens, X.-P. Wang, C.-H. Tung, D. Sun and L.-S. Zheng, *Dalton Trans.*, 2019, **48**, 3635-3640.
26. D. R. Kauffman, D. Alfonso, C. Matranga, H. Qian and R. Jin, *J. Am. Chem. Soc.*, 2012, **134**, 10237-10243.
27. M. Cowan and G. Mpourmpakis, *Dalton Trans.*, 2020, **49**, 9191-9202.
28. N. Austin, S. Zhao, J. R. McKone, R. Jin and G. Mpourmpakis, *Catal. Sci. Technol.*, 2018, **8**, 3795-3805.
29. S. Zhao, N. Austin, M. Li, Y. Song, S. D. House, S. Bernhard, J. C. Yang, G. Mpourmpakis and R. Jin, *ACS catal.*, 2018, **8**, 4996-5001.
30. M. Zhu, C. M. Aikens, F. J. Hollander, G. C. Schatz and R. Jin, *J. Am. Chem. Soc.*, 2008, **130**, 5883-5885.
31. G. Li, H. Abroshan, C. Liu, S. Zhuo, Z. Li, Y. Xie, H. J. Kim, N. L. Rosi and R. Jin, *ACS Nano*, 2016, **10**, 7998-8005.
32. Y. Song, J. Zhong, S. Yang, S. Wang, T. Cao, J. Zhang, P. Li, D. Hu, Y. Pei and M. Zhu, *Nanoscale*, 2014, **6**, 13977-13985.
33. D. R. Kauffman, J. Thakkar, R. Siva, C. Matranga, P. R. Ohodnicki, C. Zeng and R. Jin, *ACS Appl. Mater. Interfaces*, 2015, **7**, 15626-15632.
34. A. V. Nagarajan, R. Juarez-Mosqueda, M. J. Cowan, R. Jin, D. R. Kauffman and G. Mpourmpakis, *SN Appl Sci.*, 2020, **2**, 680.
35. S. Li, D. Alfonso, A. V. Nagarajan, S. D. House, J. C. Yang, D. R. Kauffman, G. Mpourmpakis and R. Jin, *ACS catal.*, 2020, **10**, 12011-12016.
36. Q. Tang, G. Hu, V. Fung and D.-e Jiang, *Acc. Chem. Res*. 2018, **51**, 2793−2802.
37. M. G. Kibria, C. T. Dinh, A. Seifitokaldani, P. De Luna, T. Burdyny, R. Quintero‐Bermudez, M. B. Ross, O. S. Bushuyev, F. P. García de Arquer and P. Yang, *Adv. Mater.*, 2018, **30**, 1804867.
38. Z. Wang, T. Li, Q. Wang, A. Guan, N. Cao, A. M. Al-Enizi, L. Zhang, L. Qian and G. Zheng, *J. Power Sources*, 2020, **476**, 228705.

TOC

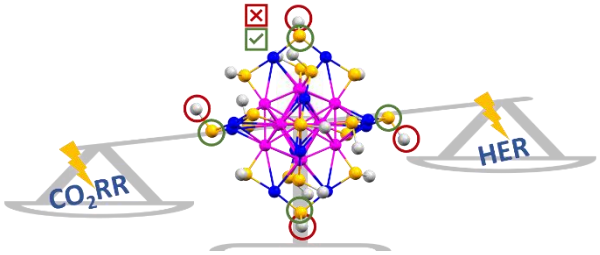

S/Se atoms at the metal-ligand interface can play an important role in determining the overall electrocatalytic performance of Au nanoclusters.